ACS APPLIED MATERIALS & INTERFACES

www.acsami.org Research Article

Accelerated Durability Assessment and a Proposed Degradation Mechanism of $NiCoO_x$ OER Catalysts under Simulated Intermittent Renewable Power: Insights from XAS

Ashraf Abdel Haleem,* Hayato Enjoji, Kyounghee Gu, Takuto Miwa, Yoshiyuki Kuroda, Yuki Orikasa, Tomoki Uchiyama, Yoshiharu Uchimoto, and Shigenori Mitsushima

Cite This: *ACS Appl. Mater. Interfaces* 2025, 17, 61929–61940 Read Online

ACCESS | Metrics & More | Article Recommendations | Supporting Information

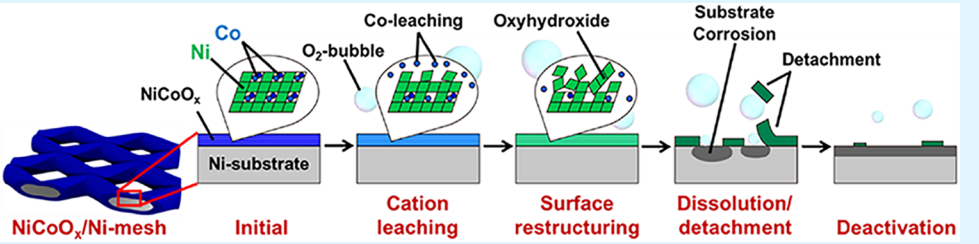

ABSTRACT: The substantial cost reductions in renewable energy sources (RES), particularly solar and wind, could facilitate their large-scale integration into modern power systems, thereby accelerating the transition toward a carbon-neutral economy. However, the inherent intermittency of RES highlights the critical need for efficient energy storage technologies, with green hydrogen emerging as a promising and sustainable energy carrier. Alkaline water electrolysis offers a scalable and cost-effective solution; however, ensuring the long-term durability of electrodes under dynamic operation remains a critical challenge. In this study, the durability of $NiCoO_x$ OER catalysts was evaluated using two accelerated degradation test (ADT) protocols: a conventional cyclic voltammetry (CV-ADT) protocol and a start-up/shut-down protocol. The latter was specifically designed to simulate the operational characteristics of (RES)-driven systems, including the effects of reverse current phenomenon typically observed in bipolar plate AWE stacks. This protocol imposed more severe stressors on the electrodes than the CV-ADT protocol, most likely providing a more realistic simulation of the intermittent conditions encountered in RES-based operation. Electrochemical measurements, along with *operando* and *ex situ* X-ray absorption spectroscopy, provided insights into the OER active sites and the degradation mechanisms of the catalyst under repeated start-up/shut-down ADT cycles. The results suggested that cobalt leaching at and beneath the electrode/electrolyte interface is a likely key factor contributing to catalyst detachment from the substrate.

KEYWORDS: *accelerated durability test, $NiCoO_x$, OER catalyst, X-ray absorption spectroscopy, degradation mechanism*

1. INTRODUCTION

Hydrogen is identified as a pivotal element in achieving net-zero emissions and sustainable development, serving as a clean energy carrier with applications across various sectors, including transportation, industry, and power generation.[1,2] As the world transitions toward a hydrogen-based society—where hydrogen plays a central role in energy systems—its production, storage, and utilization are being actively developed to replace fossil fuels and reduce carbon emissions.[3] Advancements in green hydrogen production, particularly through water electrolysis powered by renewable energy sources, are essential for realizing a sustainable hydrogen economy and accelerating the global shift toward carbon neutrality.[4,5]

With the continuous reduction in the levelized cost of electricity from renewable energy sources, particularly solar and wind, green hydrogen is increasingly regarded as a pivotal vector for facilitating the transition to a renewable energy-driven economy.[6−8] Advancements in electrolyzers efficiency, durability, and cost-effectiveness, along with improvements in system integration and scalability, will be critical for the widespread commercialization of green hydrogen production.[9] Among the various water electrolysis technologies, Alkaline Water Electrolysis (AWE) stands out as the most cost-effective, mature, and scalable solution, offering significant advantages such as low capital investment and the use of nonprecious metal catalysts.[9]

However, the intermittency of renewable energy sources (RESs) presents significant challenges, as fluctuations in power supply impose stressors on the system, potentially leading to

Received: May 29, 2025
Revised: October 21, 2025
Accepted: October 21, 2025
Published: October 29, 2025

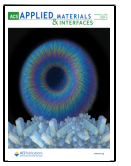

https://doi.org/10.1021/acsami.5c10518
ACS Appl. Mater. Interfaces 2025, 17, 61929−61940

durability issues and service life shortening.[10−12] One of the critical factors contributing to these challenges is the reverse current phenomenon, which can occur during transient periods of renewable energy generation.[13−16] This phenomenon subjects the electrolyzer's catalysts to frequent oxidation/reduction cycles, which, when repeated over time, can degrade the catalyst performance and reduce overall system efficiency. Understanding and mitigating stressors on catalysts are essential for enhancing the long-term stability and reliability of bipolar plate alkaline water electrolyzers under dynamic operating conditions, with sacrificial metals and self-healing approaches emerging as effective strategies to protect catalysts and extend system longevity.[17−20]

Accelerated degradation tests that realistically simulate industrial operating conditions under the inherent intermittency of RESs are crucial for developing robust electrocatalysts and enhancing the durability of water electrolyzers.[10,21] This, in turn, can reduce the operational costs of green hydrogen production, making it more cost-effective and competitive with fossil fuel-based hydrogen production.[22,23] In several studies, catalyst stability has often been assessed through bulk electrolysis at relatively low current densities for relatively short durations or by cycling the electrode potential between two set values—one representing the start-up condition and the other simulating the shutdown condition of AWE.[24] However, these approaches may not accurately replicate the harsh industrial conditions of alkaline water electrolyzers, particularly under the dynamic load variations induced by intermittent renewable power input.[25]

An Accelerated Degradation Test (ADT) protocol was developed by our team to assess electrode durability in alkaline water electrolyzers, replicating the dynamic and intermittent conditions characteristic of RES operation.[10] This protocol is based on our pioneering investigation into the reverse current behavior of Ni-based anodes, which was the first to measure the actual reverse currents in an alkaline water electrolyzer (AWE) stack and estimate their effects on electrode potentials.[16] By demonstrating how residual electromotive forces (*emfs*) of bipolar plates (BPs) during shutdown drive reduction reactions on the anode surface, inducing cathodic shifts in potential, our study laid the foundation for the development of a realistic ADT protocol.

The start-up/shut-down ADT protocol was designed to mimic realistic industrial operating conditions. It begins with a steady-state chronopotentiometry (CP) step at a rated current density, simulating continuous electrolysis under full load. This is followed by a cathodic linear sweep voltammetry (LSV) step conducted at a rapid scan rate to replicate the shutdown transition. The protocol concludes with a chronoamperometry (CA) step applied at a controlled shutdown potential (E_{OFF}). The E_{OFF} value, identified through reverse current measurements, corresponds to the minimum anode potential observed during the shutdown phase.

Our research highlighted that middle bipolar plates experience higher reverse currents compared to edge bipolar plates due to the electrolyte potential gradient. These elevated currents accelerate degradation by inducing unfavorable oxidation−reduction cycles on the electrode surfaces. The shut-down phase of E_{OFF} replicates these reduction cycles to simulate the stressors experienced during shutdown, effectively assessing the electrochemical degradation behavior. By reproducing the reverse current effects observed in real-world intermittent operation, the ADT protocol provides a robust framework for evaluating the durability of electrode materials under conditions relevant to RES-driven alkaline water electrolysis. This comprehensive approach addresses a pressing need in the field and enables the development of more resilient electrode materials for sustainable energy applications.

Building on our previous research on electrode durability in alkaline water electrolyzers under dynamic conditions, this study provides new insights into electrode active cites and degradation mechanisms. By combining electrochemical measurements, X-ray absorption spectroscopy (XAS), and comprehensive physical characterization before and after multiple cycles of the start-up/shut-down ADT protocol, we elucidated critical degradation pathways. These findings are essential for developing more robust and durable electrode materials, ultimately enhancing the long-term stability and efficiency of AWEs for sustainable hydrogen production.

2. EXPERMINTAL SECTION

2.1. Preparation of the $NiCoO_x$ OER Electrocatalyst Electrodes. The $NiCoO_x$ thin film was prepared on an expanded Ni-mesh substrate using a repeated dip-coating and thermal decomposition method. Initially, the Ni-mesh substrate was chemically etched in boiling 20% hydrochloric acid to remove surface impurities and oxides, followed by thorough rinsing with deionized water to eliminate any residual acid. Film deposition was then initiated by immersing the cleaned Ni-mesh substrate into a highly concentrated aqueous precursor solution containing nickel and cobalt salts in a 1:2 molar ratio. The substrate remained in the solution for approximately 10 s to allow uniform coating. After coating, the substrate was air-dried at 70 °C for 10 min, followed by cooling in ambient air for 10 min. Thermal decomposition was then carried out in air at 450 °C for 15 min, after which the substrate was again cooled in ambient air for 10 min. This entire process (coating, drying, cooling, thermal decomposition, and cooling) was repeated for a total of eight cycles. Following the final cycle, an additional thermal decomposition step was performed at 450 °C for 60 min to complete the fabrication process.

2.2. Electrochemical Measurements. We recently introduced standardized measurement techniques, including electrochemical half-cell and full-cell methods for AWE and PEMWE, evaluation procedures for catalytic activity and durability under both steady and dynamic operation, as well as advanced catalyst analysis using *operando* X-ray absorption fine structure (XAFS) analysis.[26] In the present study, we followed the same measurement protocols.

All electrochemical experiments were performed in a 500 mL three-electrode electrochemical cell fabricated from polytetrafluoroethylene (PTFE) to ensure chemical resistance. The working electrode (anode) consisted of a Ni-mesh (1 cm × 1 cm) uniformly coated with NiCoOx, serving as the OER electrocatalyst. A reversible hydrogen electrode (RHE) was employed as the reference electrode, while a nickel wire functioned as the counter electrode (cathode). The Ni wire was formed into a spiral with two immersed branches to increase the surface area and ensure stable HER performance at high current densities. Although Pt offers superior HER activity, it was not used to better replicate practical alkaline water electrolysis conditions. All measurements were referenced to the RHE, thereby minimizing the influence of the counter electrode on the anode potential.

The working electrode ($NiCoO_x$/Ni-mesh) was vertically mounted in the cell using a nickel wire encased in a heat-shrink plastic tube for insulation. The anode electrode had a projected

https://doi.org/10.1021/acsami.5c10518
ACS Appl. Mater. Interfaces 2025, 17, 61929−61940

area of 1 cm^2. The distance between the working electrode and the Luggin capillary of the reference electrode was maintained at approximately 1.0 cm. The nickel wire used as the cathode was chemically etched in boiling dilute hydrochloric acid for about 5 min. To prevent the electrochemically generated hydrogen from diffusing into the cell electrolyte, the cathode was enclosed in a cylindrical tube made of a Zirfon membrane.

The electrolyte used in this study was a 7.0 M aqueous KOH solution, prepared by dissolving a precise amount of KOH (Junsei Chemical Co., Ltd.) in deionized water (Milli-Q, 18 MΩ·cm). The KOH solution in the three-electrode cell was saturated with nitrogen, while the reference electrode electrolyte was saturated with hydrogen by bubbling for 20 min prior to each experiment, with bubbling continued throughout the experiments. The electrolyte temperature was maintained at 80 °C during the pretreatment (electrochemical activation) and at 25 °C during the durability testing.

All electrochemical experiments were performed using a Bio-Logic SAS potentiostat (model: VSP-300) controlled by EC-Lab software (version 11.30).

2.2.1. Cyclic Voltammetry (CV). Cyclic voltammetry measurements were conducted in a potential window of 0.5 to 2.0 V vs RHE at scan rates of 5, 50, and 150 $mV \cdot s^{-1}$ for three consecutive cycles.

2.2.2. Electrochemical Impedance Spectroscopy (EIS). Electrochemical impedance spectroscopy was performed under potentiostatic conditions (PEIS) at potential values of 1.5, 1.6, and 1.7 V vs RHE. An alternating current signal with a frequency range of 100 kHz to 100 mHz and an amplitude of 10 mV was applied during the measurements. The ohmic resistance, corresponding to the electrolyte resistance between the anode and the reference electrode, was determined from the high-frequency region of the EIS data. This resistance value was used to compensate for the *iR* drop, ensuring accurate *iR*-free potential values.

2.3. Electrochemical Pre-Treatment of the Electrocatalysts. Before conducting the ADT experiments, the as-prepared samples underwent electrochemical pretreatment to enhance their OER activity. This pretreatment process, also referred to as aging or conditioning, was performed by carrying out water electrolysis under a DC current density of 1.0 A cm^{-2} for 2 h at a temperature of 80 °C. Subsequent electrochemical characterizations of the anode were conducted to evaluate the effectiveness of the pretreatment conditions in improving its performance. It is worth noting that the catalytic activity of the catalyst-coated Ni mesh substrate is significantly enhanced compared to the bare Ni mesh, particularly in the high-potential region relevant to our durability study (Figure S1). This confirms that the contribution of the underlying Ni mesh to the OER activity is negligible prior to significant degradation during ADT testing.

2.4. Accelerated Degradation Test Protocols. The $NiCoO_x$/Ni-mesh catalysts for the oxygen evolution reaction were evaluated using two distinct ADT protocols: (a) a start-up/shut-down ADT, as illustrated in Figure S2a, and a cyclic voltammetry-based ADT (CV-ADT), shown in Figure S2b.

2.4.1. Overview of the Proposed Start-up/Shut-down ADT Protocol. This ADT protocol emulates the operating conditions of industrial alkaline water electrolyzers derived by intermittent renewable energy sources, with a focus on the reverse current effects during shutdown. It mainly consisted of two phases:

- Steady-state electrolysis phase (CP Step): Each ADT cycle begins with chronopotentiometry at a constant current density of 0.6 $A \cdot cm^{-2}$ for 1.0 min. This step represents the steady-state operation of the electrolyzer under continuous power supply.
- Electrolysis shut-down phase (LSV and CA Steps): After the steady-state operation, a cathodic linear sweep voltammetry (LSV) step is applied with a fast sweep rate (ν) to simulate rapid power fluctuations. This is followed by a chronoamperometry (CA) step at a controlled potential (E_{OFF}).

The value of E_{OFF} is derived from our prior investigations into the reverse current phenomenon of Ni-based anodes. During shutdown, the reverse current generated by the residual electromotive forces (emfs) of the bipolar plates (BPs) drives reduction reactions on the Ni-based anodes. These reduction reactions are reflected in the cathodic shifts of the anode potential, as previously reported. By carefully analyzing the behavior of the anode potential under reverse current conditions, E_{OFF} was selected to replicate these reductions and simulate the stressors experienced by the anode during shutdown. This ensures that the ADT protocol is highly likely to effectively mimic the electrochemical degradation mechanisms relevant to real-world intermittent operation.

2.4.2. Relevance of the Start-up/Shut-down ADT Protocol to the Reverse Current Phenomenon. The start-up/shut-down ADT protocol is directly informed by the reverse current behavior observed in alkaline water electrolyzers during shutdown. Our previous study demonstrated that the reverse currents are initially high, driven by the discharge of accumulated charges on the electrodes.[13−16] These currents gradually decrease as the electrolyte potential equalizes across the stack. Middle bipolar plates experience higher reverse currents due to the electrolyte potential gradient, which accelerates degradation by inducing unfavorable oxidation and reduction cycles at the electrode surfaces. The CA step at E_{OFF} specifically reproduces these reduction cycles to evaluate their impact on electrode durability.

2.4.3. Design of the Conventional Cyclic Voltammetry ADT (CV-ADT) Protocol. The electrode potential was repeatedly cycled between two defined values: 1.8 V vs RHE (E_{max}), simulating the start-up condition, and 0.3 V vs RHE (E_{min}), representing the shutdown condition of an alkaline water electrolyzer (AWE). The sweep rate was set to 1.0 V s^{-1}, and the cycling was continued for a total of 40,000 cycles.

2.5. Electrochemical Characterization. To monitor electrode performance and degradation, cyclic voltammetry (CV) and electrochemical impedance spectroscopy (EIS) measurements were performed after every 200 cycles of the start-up/shut-down ADT protocol. In addition, the electrode potential versus RHE was recorded during the steady-state electrolysis phase at 600 mA cm^{-2} in each ADT cycle. The corresponding *iR*-corrected values were calculated using the average solution resistance, determined from EIS measurements conducted after every 200 ADT cycles. These corrected potentials, along with the evolution of CV responses throughout the ADT process, were collectively used to assess the extent of electrode degradation or stability over time. The full ADT experiment consisted of 2000 cycles, divided into 10 groups of 200 cycles each. Including all electrochemical measurements, the total experiment duration was approximately 70 h.

https://doi.org/10.1021/acsami.5c10518
ACS Appl. Mater. Interfaces 2025, 17, 61929−61940

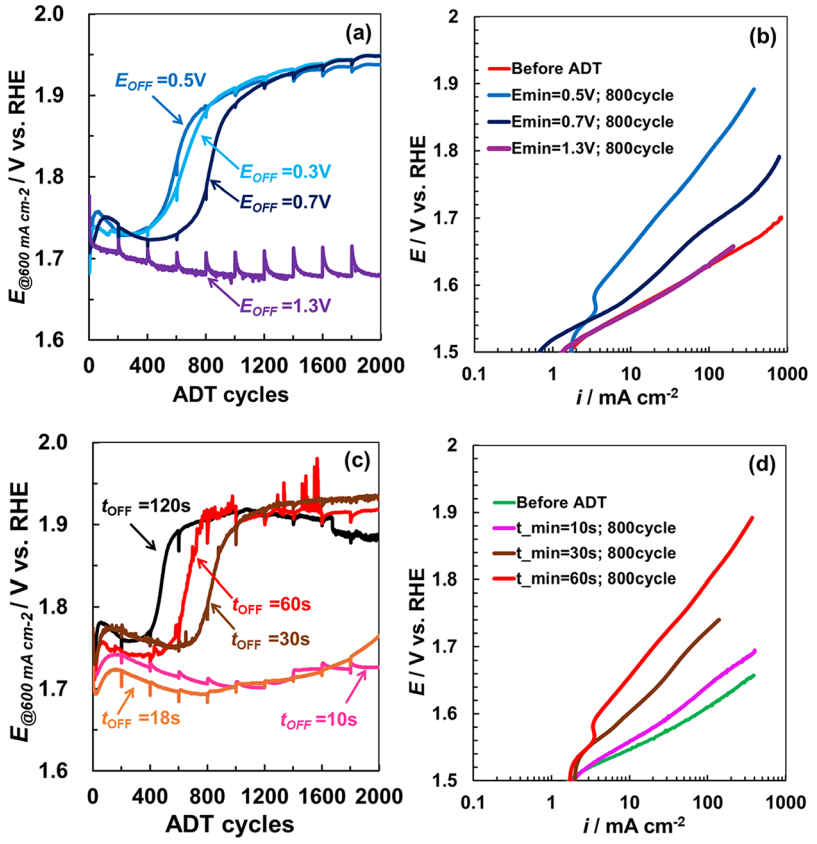

Figure 1. (a) Electrode potentials recorded at 600 mA cm^{-2} during start-up/shut-down ADT cycles at different shut-down potentials E_{OFF} = 0.3, 0.5, 0.7, and 1.3 V vs RHE, each with a fixed shut-down duration t_{OFF} = 60 s, (b) Corresponding polarization curves, at ν = 5 mV s^{-1}, for selected samples that exhibited distinct behaviors, (c) Electrode potentials at 600 mA cm^{-2} under ADT cycles with varying shut-down durations t_{OFF} = 10, 18, 30, 60, and 120 s at a fixed shut-down potential of E_{OFF} = 0.5 V vs RHE, (d) Corresponding polarization curves, at ν = 5 mV s^{-1}, for selected samples that exhibited distinct behaviors.

By integrating the insights from reverse current behavior and tailoring E_{OFF} to the observed reductions of Ni-based anodes, the ADT protocol provides a robust framework for assessing the long-term durability of electrodes in alkaline water electrolyzers under realistic conditions.

2.6. Crystalline Structure Characterization. The crystalline structure of the freshly prepared film was characterized by X-ray diffraction (XRD) using a Rigaku Ultima IV diffractometer, as shown in Figure S3. The XRD pattern indicated that the dominant phase is $NiCo_2O_4$ with a spinel structure, while minor diffraction peaks corresponding to NiO were also observed. Phase identification was carried out by comparing the diffraction patterns with standard reference data: PDF #20-0781 for $NiCo_2O_4$ and JCPDS #47-1049 for NiO.

2.7. *Ex situ* and *Operando* Measurements. *Operando* Co and Ni K-edge XAS measurements were conducted at beamline BL37XU at SPring-8, Japan. The experimental setup for the *operando* measurements included a Pt rod as the counter electrode, a RHE as the reference electrode, and N_2-saturated 7.0 M KOH as the electrolyte. The $NiCoO_x$ electrode was used as the working electrode, which was coated on a titanium substrate. To examine electronic structural changes during the OER, XAS data were collected at different potentials (vs RHE) and various incident angles. To minimize scattering from the electrolyte solution, the sample was positioned close to a Kapton film X-ray window during measurements. All experiments were performed at room temperature.

Ex situ Co L-, Ni L-, and O K-edge X-ray absorption near-edge structure (XANES) spectra were obtained in total electron yield (TEY) and partial fluorescence yield (PFY) modes at the Ritsumeikan University SR Center (beamline BL-11) and Aichi Synchrotron Radiation Center (BL1N2). For each edge, background subtraction in the pre-edge region and postedge normalization were performed to ensure high accuracy and reproducibility in the spectral analysis. Specifically, data points near 770 and 805 eV were used for the Co K-edge, 830 and 870 eV for the Ni K-edge, and 523 and 570 eV for the O K-edge to define the pre-edge and postedge regions, respectively. While *operando* soft XAS is a powerful technique for probing the electronic structure of electrocatalysts under realistic working conditions, its implementation typically requires custom-designed cells, specialized window materials, and specific electrode geometries that may not reflect the practical configurations or materials used in standard electrolysis systems.[27] In this study, soft XAS measurements were conducted under vacuum conditions, which differ from the actual electrochemical environment, particularly with respect to hydration and surface adsorbates present during operation.[28] Therefore, we utilize *ex situ* soft XAS data to assess the degradation state of the catalyst, rather than to directly track its electrochemical behavior under *operando* conditions.

3. RESULTS AND DISCUSSION

3.1. Accelerated Durability Testing Experiments. As shown in Figure S4a, the electrode potential of the $NiCoO_x$/Ni-

https://doi.org/10.1021/acsami.5c10518
ACS Appl. Mater. Interfaces 2025, 17, 61929−61940

mesh OER catalyst at 10 mA cm^{-2} increased slightly after 40,000 cycles under the CV-ADT protocol, while a pronounced rise was observed after just 2000 cycles under the start-up/shut-down ADT protocol. This result was confirmed by the CV measurements of the initial samples as well as those subjected to the CV-ADT and start-up/shut-down tests, as shown in Figure S4b,c, respectively. Correspondingly, the Tafel slope increased from an initial value of ~56 to 69.5 mV dec^{-1} after CV-ADT and to ~155 mV dec^{-1} after the start-up/shut-down ADT, as shown in Figure S4d. These results indicate that the catalyst maintained high stability during CV-ADT over extended cycling, whereas it suffered rapid degradation under the start-up/shut-down protocol. These contrasting results highlight the pronounced impact of dynamic operating conditions on catalyst durability and underscore the importance of tailoring stability assessments to realistic electrolysis scenarios.[10,21,25,29]

For the start-up/shut-down ADT protocol, the electrode potential (E_{OFF}) and the duration (t_{OFF}) of the voltage-controlled step representing the shutdown phase must be carefully selected to simulate real-world conditions. Specifically, the electrode potential during shutdown should be maintained significantly below the open-circuit potential (*OCP*) of the electrode. This ensures complete reduction of the electrode surface material due to the reverse current flowing between the anode and cathode on the same bipolar plate through the metallic bipolar plate and the ionically conducting electrolyte in the manifolds, as demonstrated in our previous study on the reverse current phenomenon.

Figure 1a illustrates the electrode potential under 600 mA cm^{-2} of electrolysis current as a function of ADT cycles, tested with t_{OFF} = 60 s and E_{OFF} = 0.3, 0.5, 0.7, and 1.3 V vs RHE. In this figure, the electrode potential for each ADT cycle represents the average value recorded during the 60-s steady-state electrolysis at 600 mA cm^{-2} (the chronopotentiometry step of the start-up/shut-down ADT protocol), reflecting the measured potential for each cycle. After 200 cycles, the test was briefly interrupted for electrochemical characterization (cyclic voltammetry and impedance), causing minor changes in electrode potential upon resuming, likely due to double-layer charging and discharging currents. Notably, for E_{OFF} = 0.3 and 0.5 V vs RHE, the degradation began after approximately 400 ADT cycles, whereas increasing E_{OFF} to 0.7 V vs RHE delayed the onset of degradation to roughly 600 cycles. In addition, Figure 1b shows the corresponding polarization curves for samples selected from Figure 1a after 800 ADT cycles at a sweeping rate of ν = 5 mV s^{-1}, highlighting samples with distinct durability behaviors. A rapid decline in electrode OER performance was observed under ADT when E_{OFF} was between 0.3 and 0.7 V vs RHE. In contrast, at E_{OFF} = 1.3 V vs RHE, the electrode demonstrated notable durability. Its polarization curve remained largely unchanged compared to that of the as-prepared sample, unlike the pronounced deviations observed at 0.5 and 0.7 V vs RHE. This result is further supported by the polarization curves of the samples tested at E_{OFF} = 0.5 V vs RHE and E_{OFF} = 1.3 V vs RHE, as shown in Figure S5a,b, respectively. These findings suggest that applying appropriate electrode potentials during electrolysis interruption periods can significantly influence catalyst durability under intermittent electrolysis conditions.

This result can be interpreted based on our previous investigation into the reverse current phenomenon, which revealed that the potential of the $NiCoO_x$-based anode dropped to approximately 0.55 V vs RHE after 30 min of shutdown. Such low potential and the associated reduction reactions of the anode material contributed to the rapid decline in OER performance after multiple cycles, as corroborated by the current start-up/shut-down ADT results. When E_{OFF} was maintained at 0.5 V vs RHE, the oxidation peaks of the active species—initially observed at 1.3−1.35 V vs RHE—gradually diminished and eventually disappeared as the ADT progressed. Simultaneously, new oxidation peaks emerged at higher potentials (1.4−1.45 V vs RHE), potentially corresponding to the oxidation of the Ni substrate, as shown in Figure S6a. In contrast, when E_{OFF} = 1.3 V vs RHE, the oxidation peaks of the active species remained stable, and no oxidation peaks attributable to the Ni substrate were observed, as illustrated in Figure S6b. This stability is consistent with the sustained OER performance of the electrode under this relatively positive shutdown potential, which was close to the *OCP* of the electrode.

Furthermore, the durability of the samples was evaluated at E_{OFF} = 0.5 V vs RHE with varying shutdown durations (t_{OFF}) of 10, 18, 30, 60, and 120 s. The electrode potentials under a current density of 600 mA cm^{-2} as a function of ADT cycles for the tested samples are presented in Figure 1c. The results highlighted the significant influence of the shutdown duration (t_{OFF}) of the start-up/shut-down ADT protocol on electrode durability. For t_{OFF} = 10 and 18 s, no substantial impact on electrode durability was observed. However, longer shutdown durations (t_{OFF} = 30, 60, and 120 s) led to a pronounced degradation of the OER performance of the tested electrodes. The onset of degradation varied with t_{OFF}, occurring earlier as the shutdown duration increased, indicating a progressive negative effect of extended t_{OFF} on electrode durability. In addition, the polarization curves, at a sweeping rate of ν = 5 mV s^{-1}, of samples tested at t_{OFF} durations of 10, 30, and 60 s over 800 ADT cycles confirmed that the deviation in behavior from the as-prepared sample increased with longer shutdown durations. The impact of shut-down duration on electrode degradation behavior is further evidenced by the polarization curves of samples subjected to varying t_{OFF} values, as presented in Figure S7a−c. These findings indicate that the stressors affecting the electrodes during start-up/shut-down operation are determined not only by the electrode potential during the shutdown phase but also by the duration for which the electrode remains at that potential.

Ultimately, the start-up/shut-down ADT protocol imposed severe stress conditions that closely resemble those encountered during operation under intermittent renewable energy sources (RESs). Moreover, it offers a time-efficient and promising approach for evaluating catalyst durability under realistic scenarios.

3.2. X-ray Absorption Spectroscopy Measurements.

To avoid interference from the Ni substrate in the original $NiCoO_x$/Ni-mesh electrode, *ex situ* hard XAS and *operando* measurements were carried out on $NiCoO_x$-coated Ti plates to investigate the oxidation states of Ni and Co in the catalyst. The CV measurements (Figure S8a,b) showed that $NiCoO_x$ on both Ni mesh and Ti plate exhibited similar initial oxidation peak potentials, indicating comparable intrinsic activity and minimal substrate influence due to the sufficient film thickness. ADT measurements were performed on Ni-mesh substrates, representative of industrial alkaline anodes, as they provide high conductivity and strong catalyst adhesion. However, The $NiCoO_x$/Ti samples were not subjected to long-term ADT testing but were used exclusively to isolate the catalyst's intrinsic spectroscopic features, in *operando* XAS measurements, without

https://doi.org/10.1021/acsami.5c10518
ACS Appl. Mater. Interfaces 2025, 17, 61929−61940

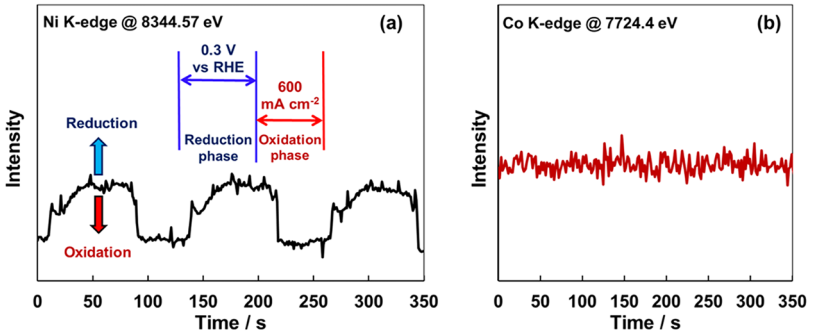

Figure 2. *Operando* XANES intensity at (a) the Ni K-edge (8344.57 eV) and (b) the Co K-edge (7724.4 eV) as a function of time during start-up/shut-down ADT cycling in 7.0 M KOH.

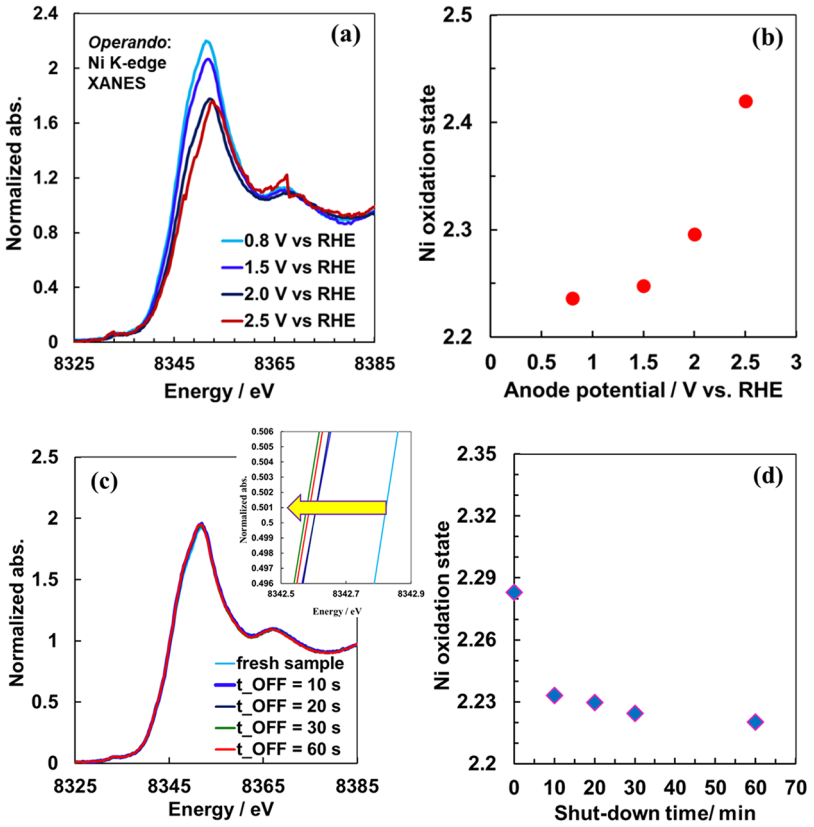

Figure 3. *Operando* Ni K-edge XANES spectra at electrode potential of 0.8, 1.5, 2.0, and 2.5 V vs RHE (a), Estimated Ni oxidation state from the energy of the first inflection point using NiO and NiOOH as Ni^{2+} and Ni^{3+} references versus the anode potential (b), *operando* Ni K-edge XANES spectra in case of t_{OFF} = 0, 10, 20, 30, 60 s (the inset shows the spectra at about normalized absorption of 0.5) (c), and Estimated Ni oxidation state from the energy of the first inflection point using NiO and NiOOH as Ni^{2+} and Ni^{3+} references versus the shut-down time t_{OFF} (d).

interference from the Ni substrate. Reference samples, including NiO (Ni^{2+}), NiO(OH) (Ni^{3+}), and Co_3O_4 (a mixture of Co^{2+} and Co^{3+}), were measured under the same conditions as the $NiCoO_x$/Ti sample. The XANES spectra at the Ni K-edge and Co K-edge for both the $NiCoO_x$ and reference samples are presented in Figure S9a,b, respectively. The XANES spectra revealed that the Ni ion in $NiCoO_x$/Ti consisted of both Ni^{2+} and Ni^{3+} species, as the intensity and position (in eV) of the main absorption peak were intermediate between those of the Ni^{2+} and Ni^{3+} oxidation states. Notably, the absorption peak at Ni K-edge in the $NiCoO_x$/Ti sample was slightly closer to that of the Ni^{3+} species, indicating that Ni^{3+} predominantly represented the oxidation state of Ni in the catalyst electrode. In addition, the Co K-edge XANES revealed that the electronic state and bonding symmetry of cobalt in $NiCoO_x$/Ti were like those of Co_3O_4, suggesting that cobalt existed in a mixed-valence state of +2 and +3.[30,31]

By monitoring the X-ray absorption intensity at a specific energy point near the absorption edge—where significant changes in intensity occur—it is possible to track variations in the oxidation state of the same sample over time. The *operando* intensity changes at Ni K-edge (8344.57 eV) and Co K-edge (7724.4 eV) for the $NiCoO_x$/Ti electrode were recorded under multiple start-up/shut-down ADT cycles. The start-up phase involved operation at a current density of 600 mA cm^{-2} for 1 min, while the shut-down phase consisted of a linear sweep voltammetry (LSV) scan at −500 mV s^{-1}, followed by a constant electrode potential of 0.3 V vs RHE for 1 min in 7.0 M KOH.

https://doi.org/10.1021/acsami.5c10518
ACS Appl. Mater. Interfaces 2025, 17, 61929−61940

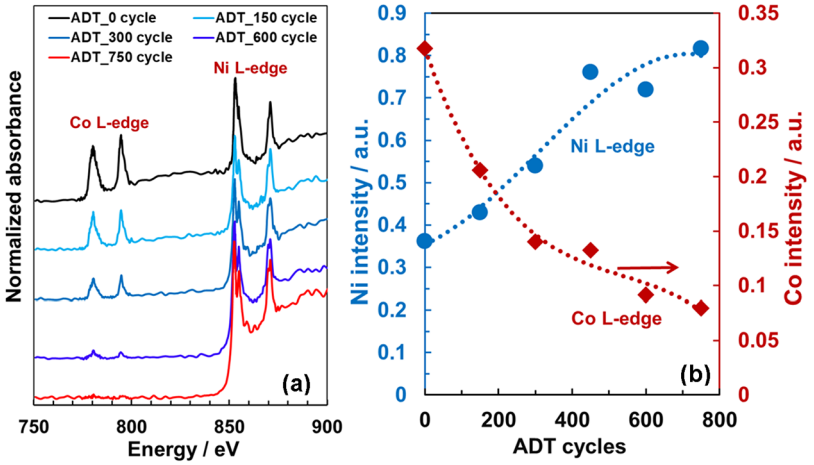

Figure 4. (a) *Ex situ* Co L-edge and Ni L-edge X-ray absorption spectra of the $NiCoO_x$/Ni electrode. (b) Integrated Co and Ni intensities, calculated from the peak areas within the energy ranges of 776−786 eV and 840.6−857.8 eV, respectively.

The Ni K-edge intensity, shown in Figure 2a, exhibited a clear response to the applied potential. During the water oxidation process, the absorption edge intensity decreased, indicating the oxidation of Ni species. Upon transitioning to the shut-down step, where a reducing potential of 0.3 V vs RHE was applied, the absorption edge intensity increased again, reflecting the reduction of Ni species. This reversible behavior confirms that Ni undergoes oxidation and reduction cycles in response to potential variations.

In contrast, the intensity of Co K-edge (~7724.4 eV), shown in Figure 2b, remained unchanged throughout the start-up/shut-down ADT cycles, showing no noticeable shift in the absorption edge intensity. This indicates that the oxidation state of Co remained largely stable, existing as a Co^{2+}/Co^{3+} mixture without significant redox transitions during the oxygen evolution reaction (OER). Unlike Ni, which exhibited clear redox activity, Co did not respond to the applied potential, suggesting its limited direct involvement in the OER mechanism.[32]

These results suggest that Ni-based species play a pivotal role as the primary active sites for the OER, while Co contributes synergistically to enhance the catalytic performance of Ni active sites but is not directly involved in the redox-driven OER process.[32] In addition, *operando* Ni K-edge XANES spectra were recorded for the $NiCoO_x$/Ti sample at various oxidation potentials—0.8, 1.5, 2.0, and 2.5 V vs RHE—each maintained for approximately 30 min prior to spectral acquisition in 7.0 M KOH, shown in Figure 3a. As the applied potential increases, the Ni K-edge shifts to higher energy, accompanied by a decrease in white-line intensity. This behavior is consistent with the reported formation of NiOOH, which alters the local electronic structure and coordination environment of Ni species.[33] At the Ni K-edge, the white line originates from the 1s → 4p transition. Because Ni 4p orbitals are generally unoccupied, its intensity is not expected to vary strongly with oxidation state alone. In the literature, changes in white-line intensity are often accompanied by a concurrent edge shift.[33] In contrast, our *operando* XANES spectra showed a pronounced decrease in white-line intensity above 1.5 V vs RHE, without a corresponding significant edge shift. This indicates that the effect cannot be attributed solely to changes in the Ni oxidation state. At high anodic potentials, excess charge may be accommodated by the oxygen sublattice, leading to ligand-hole formation and increased Ni−O covalency, which in turn reduces the effective Ni 4p contribution.[28] Simultaneously, structural modifications such as local disorder, oxygen-vacancy formation, and partial transformation into NiOOH-like phases are likely to occur, as reported in theoretical and *operando* XAFS studies.[34,35] These processes reduce the Ni−O coordination number and further attenuate the white-line intensity.[36] Overall, the observed decrease in white-line intensity is best explained by the combined influence of electronic and structural effects, rather than oxidation-state changes alone. The absorption edge energy of normalized XANES intensity at 0.5, denoted as E_0, exhibited a gradual increase with increasing electrode potential as shown in Figure S10a. In addition, we identified the energy position of the first inflection point in the XANES spectra and converted it to the apparent Ni oxidation state, as shown in Figure 3b. The results indicated a progressive oxidation of Ni species at the electrode surface with increasing applied potential, reaching up to 2.5 V vs RHE. These results revealed a gradual transformation of Ni species from Ni^{2+} (present in NiO and/or $Ni(OH)_2$), which are relatively inactive for the oxygen evolution reaction (OER), to Ni^{3+} (in the form of NiOOH), which is significantly more active for OER. This oxidation process highlights the critical role of Ni^{3+} species in enhancing the catalytic performance of $NiCoO_x$ during water oxidation.[32]

Furthermore, the $NiCoO_x$/Ti sample was subjected to the start-up/shut-down ADT protocol, where the start-up step involved operation at 450 mA cm^{-2}, and the shut-down step consisted of holding the electrode at 0.5 V vs RHE for varying durations (t_{OFF} = 10, 20, 30, and 60 s). *Operando* Ni K-edge XANES spectra were recorded during both the start-up and shut-down steps of the ADT protocol, as shown in Figure 3c. The absorption edge energy of E_0, corresponding to the normalized XANES intensity at 0.5, exhibited a gradual decrease with increasing shut-down duration, as illustrated in Figure S10b. A progressive reduction of Ni species at the electrode surface was evident as the shut-down period extended, with a pronounced decrease observed up to t_{OFF} = 30 s. The estimated Ni oxidation state, derived from the first inflection point, is also shown in Figure 3d. The observed shift indicates a progressive reduction of Ni species at the electrode surface with increasing shut-down duration, with a pronounced decrease up to t_{OFF} = 30 s. These results suggest that after t_{OFF} of 30 s, most Ni species on

https://doi.org/10.1021/acsami.5c10518
ACS Appl. Mater. Interfaces 2025, 17, 61929−61940

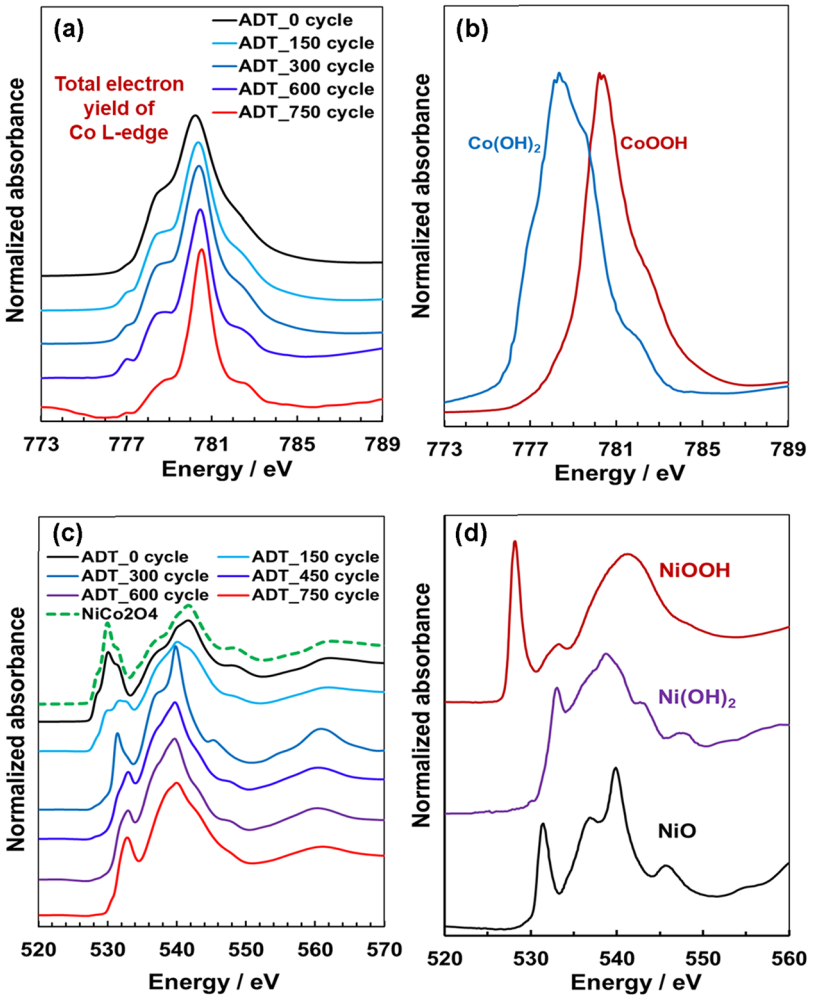

Figure 5. *Ex situ* TEY spectra at Co L-edge for the freshly prepared sample and those subjected to different cycles of the start/stop ADT protocol (a), along with reference spectra of Co $(OH)_2$ and CoOOH for comparison (b). TEY spectra at O K-edge for the freshly prepared sample and those subjected to different cycles of the start-up/shut-down ADT protocol (c), along with reference spectra of NiO, Ni $(OH)_2$ and NiOOH for comparison (d).

the electrode surface underwent a transition from Ni^{3+} (NiOOH) to Ni^{2+} (NiO and/or Ni $(OH)_2$).

To comprehensively investigate the impact of start-up/shut-down ADT cycle progression on the $NiCoO_x$/Ni electrode material, *ex situ* soft X-ray absorption measurements were conducted at different stages of OER performance degradation. These measurements were performed on both freshly prepared samples and those subjected to varying numbers of ADT cycles—specifically 150, 300, 450, 600, and 750 cycles—corresponding to different degrees of electrode degradation as shown in Figure S11. It is worth mentioning that *operando* hard XAS experiments were performed on $NiCoO_x$-coated Ti substrates to probe the intrinsic redox behavior of Ni and Co without interference from the Ni support. These Ti-based measurements were limited to short-term studies, where catalyst adhesion is less critical. In contrast, *ex situ* soft XAS of electrodes subjected to accelerated durability testing was carried out exclusively on Ni-mesh substrates, representative of industrial alkaline anodes due to their high conductivity and strong catalyst adhesion. This approach captures practical degradation phenomena, with the observed increase in Ni L-edge intensity during ADT reflecting catalyst detachment and exposure of the Ni substrate rather than a spurious artifact.

It should be noted that the Ni and Co L-edge soft-XAS spectra in this study were collected under ultrahigh vacuum (UHV) conditions. Such measurements can remove interfacial water and weakly bound adsorbates, potentially altering the apparent oxidation state compared to the hydrated state during electrochemical operation. Similar limitations have been highlighted in ambient-pressure XPS studies,[37] and *operando* soft-XAS studies have further demonstrated that key spectral features, such as the O K-edge prepeak at ∼529 eV and the Ni L_3-edge shoulder, evolve only under applied potential and hydration.[28] In this work, therefore, *ex situ* soft XAS is interpreted primarily as a post-mortem probe of degradation, while conclusions regarding the active phase evolution are based on *operando* hard XAS data.

Figure 4a presents the fluorescence X-ray absorption spectra at Co and Ni L-edges. The data showed a progressive decrease in the intensity of the Co L-edge absorption peaks, while the Ni L-edge peak intensity gradually increases with increasing ADT cycles. To evaluate these variations, the peak areas within the energy ranges of 776−786 eV (Co L-edge) and 840.6−857.8 eV (Ni L-edge) were integrated as indicators of material retention on the electrode after different numbers of ADT cycles. The results are shown in Figure 4b. The decrease in Co L-edge

https://doi.org/10.1021/acsami.5c10518
ACS Appl. Mater. Interfaces 2025, 17, 61929−61940

intensity indicates that Co species leached into the electrolyte.[30,31,38] It is worth noting that after up to 750 ADT cycles, the depletion of Co in the catalyst material is significant but not complete, as shown in Figure 4b and the Co L_3-edge spectra collected in partial fluorescence yield (PFY) mode that shown in Figure S12, which display a barely detectable Co L_3-edge peak at 750 cycles. Meanwhile, the simultaneous increase in Ni L-edge intensity suggests that not only did Co leach out, but the overall $NiCoO_x$ catalyst layer also gradually degraded, leading to increased exposure of the underlying Ni substrate. This trend suggests that the degradation mechanism involves both preferential Co leaching and the progressive detachment and/or dissolution of the catalyst layer itself.[30] The continuous loss of Co likely destabilized the catalyst structure, further accelerating the overall degradation of $NiCoO_x$/Ni and reducing its long-term stability for OER. The normalized *ex situ* TEY spectra at the Co L-edge for the freshly prepared sample and those subjected to various cycles of the start-up/shut-down ADT protocol are shown in Figure 5a. It is important to note that these normalized spectra primarily reflect changes in the Co oxidation states rather than the absolute residual Co content in the catalyst material as ADT testing progresses. Comparison with the reference spectra of Co $(OH)_2$ and CoOOH, shown in Figure 5b, indicates that the oxidation state of the remaining cobalt species in the electrode remains unchanged throughout ADT cycling. The cobalt exists primarily as a mixture of Co^{2+} and Co^{3+}, with Co^{3+} being the dominant species, as evidenced by the relative peak intensities. In fact, for a simple binary mixture, Co L-edge XANES spectra could be approximated as a linear combination of Co $(OH)_2$ (Co^{2+}) and CoOOH (Co^{3+}) reference spectra. However, the electrodes studied are more complex, so this fitting only offers semiquantitative insight. Up to 450 ADT cycles, the Co^{3+} fraction is estimated at about 80%. Beyond 600 cycles, decreased Co L-edge intensity limited reliable fitting. Transition metal L-edge spectra reflect complex electronic and ligand-field effects, making peak assignment to specific oxidation states unreliable.[39] Thus, we assess oxidation state changes by direct comparison with reference spectra for a more qualitative and accurate interpretation. However, the unnormalized *ex situ* TEY spectra at the Co L-edge for the same samples, presented in Figure S13, reveal that Co content at the electrode surface is significantly, though not completely, reduced after 750 cycles. Furthermore, the *ex situ* TEY spectra at O K-edge for the freshly prepared sample and those subjected to different cycles of the start-up/shut-down ADT protocol (Figure 5c), along with reference spectra of CoOOH, Co $(OH)_2$, and NiO (Figure 5d), reveal changes in the spectra after 450 cycles. Specifically, the spectral features associated with the spinel $NiCo_2O_4$ structure gradually transition to those resembling Ni $(OH)_2$ after 450 cycles. This Ni $(OH)_2$-like signal may originate from the Ni substrate, suggesting catalyst thinning and depletion due to prolonged ADT cycling.

X-ray photoelectron spectroscopy (XPS) measurements were performed to analyze the surface composition and oxidation states of the electrode material, and how these changes upon the accelerated degradation testing, *ex situ* XPS measurements were carried out on both the freshly prepared electrode and the sample subjected to 600 start-up/shut-down cycles. The Ni 2p and Co 2p spectra are shown in Figure S14a–c. After applying a Shirley background subtraction and integrating the $2p_3/_2$ peaks, the atomic Ni:Co ratio was determined to be 32:68 for the initial electrode, in good agreement with the nominal composition of the precursor material (Ni:Co = 1:2). Following 600 ADT cycles, this ratio shifted markedly to 86:14, indicating a substantial loss of cobalt from the electrode surface. This result is consistent with the reduction in Co L-edge intensity observed in the XANES measurements (Figures S12 and S13), thereby supporting the validity of our spectroscopic interpretations.

In terms of oxidation states, analysis of the Ni 2p spectrum was hindered by the presence of overlapping shakeup satellite features and the coexistence of local (Ni_A) and nonlocal (Ni_B) screening effects.[40] These features prevented reliable deconvolution of the Ni^{2+} and Ni^{3+} components, rendering valence-state assignment from Ni 2p XPS inconclusive. In contrast, the initial Co 2p spectrum exhibited a prominent peak at ~780 eV, which is characteristic of Co^{3+} as the dominant surface species.[40] After 600 cycles, the Co 2p signal decreased significantly, and the remaining intensity was insufficient to derive a meaningful Co^{2+}/Co^{3+} ratio.

3.3. Insights into the OER Performance Degradation Mechanism. Figure S15a presents the transient reverse current observed during the shutdown period of a single cycle in the start-up/shut-down ADT protocol. The sharp peak appearing immediately after shutdown is attributed to the nonfaradaic discharge current of the double-layer capacitance at the electrode–electrolyte interface. In contrast, the broader peak that emerges approximately 1.0 s after the onset of the shutdown potential corresponds to the faradaic current associated with the reduction of the electrode material. This faradaic current gradually decreases over the shutdown period, reflecting the progressive reduction of the electrode material. Once the reduction of the surface material is complete, the current diminishes to zero. Figure S15b shows the reverse charge, obtained by integrating the area under the transient reverse current curve, along with the electrode potential at a current density of 600 mA cm^{-2} as a function of ADT cycles. The data from this Figure is replotted in Figure S15cwith a logarithmic scale for the horizontal axis (number of ADT cycles) to emphasize the changes in the reverse charge and the electrode potential during the early stages of the test. During the initial stage (St1) of the ADT cycles, it seems that the gradual dissolution of the catalyst material increased the surface porosity, leading to a relative improvement in OER performance. This was reflected in the increased reverse charge observed during shutdown, indicating an expanded electrochemically active surface area due to enhanced porosity. The preferential leaching of Co during the initial stage of the ADT cycles (St1) may contribute to the enhanced OER performance by exposing additional Ni active sites to the electrolyte. Cobalt metal is likely not sufficiently resilient to endure the repeated structural changes associated with the oxidation and reduction cycles of the near-surface material induced by the start-up/shut-down operation.[41] In addition, cobalt's low cohesive energy makes it highly susceptible to spontaneous interactions with its environment, rendering it prone to dissolution under the highly oxidative conditions present in this experiment.[42] This Co dissolution under dynamic OER conditions may generate surface cation vacancies and structural defects, which alter the local coordination environment and increase surface reactivity, thereby facilitating improved catalytic activity.[41,43–45] However, in the second stage (St2), after approximately 20 cycles, continuous Co ion leaching can deteriorate the structural framework near the surface, causing partial collapse of the near-surface crystalline matrix and weakening of the electrode material.[45] This structural degradation reduces the mechanical stability of the catalyst layer and results in noticeable material

https://doi.org/10.1021/acsami.5c10518
ACS Appl. Mater. Interfaces 2025, 17, 61929–61940

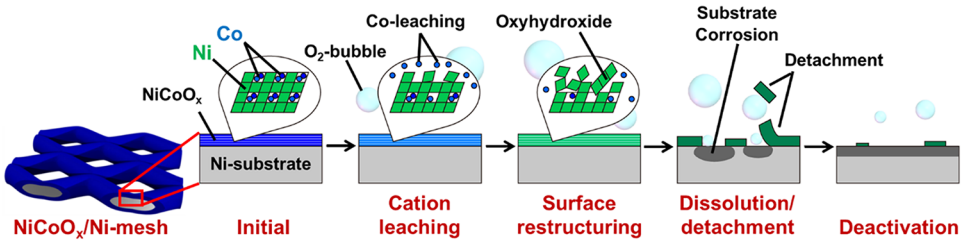

Figure 6. Schematic diagram of the degradation steps of the NiCoOx catalyst under repeated cycles of the start-up/shut-down ADT protocol.

loss during prolonged dynamic operation. This marked the onset of OER performance degradation. Notably, the mechanical stress exerted by evolving oxygen bubbles may result in the detachment of structurally weakened material from the electrode surface.[30] In the third stage (St3), up to approximately 400 ADT cycles, the reverse charge and OER performance exhibited relative stability, suggesting a temporary balance between material dissolution and surface activation. However, in the fourth stage (St4), ongoing material loss caused pronounced film thinning and a sharp decline in OER performance, as evidenced by the rapid drop in reverse charge indicating substantial catalyst depletion. Finally, in the fifth and final stage (St5), most of the catalyst material appeared to be depleted from the substrate. The remaining OER activity was likely attributed to the underlying Ni substrate, rather than the original catalyst film. Figure S16a–c shows optical images of NiCoO$_x$/Ni-mesh electrodes at different stages of the start-up/shut-down ADT: the fresh electrode before testing, after 400 ADT cycles, and after 2000 ADT cycles. Progressive discoloration and visible material-loss with an increasing number of cycles indicate cumulative structural degradation and material detachment from the electrode surface under dynamic operating conditions. Detached catalyst material was observed as dark precipitates that accumulated at the bottom of the beaker following the ADT experiments.

3.3.1. Cobalt Leaching Identified as a Key Degradation Mechanism: Evidence from ICP-OES Analysis. In a control experiment, catalyst particles detached into the electrolyte were collected using vacuum-assisted filtration through a 0.2 μm pore-size membrane, followed by thorough washing and drying. The recovered solids were dissolved in 12 M HCl and then diluted to 1.0 M HCl for analysis. Inductively coupled plasma optical emission spectrometry (ICP-OES; Shimadzu, ICPE-9000) measurements revealed a Ni:Co molar ratio of 1:1.4 in the detached particles. This composition differs markedly from that of the as-prepared and annealed NiCoO$_x$ catalyst powder measured with X-ray fluorescence spectroscopy (XRF; JEOL, JSX-3100R II), which had a Ni:Co ratio of 1:2, consistent with the initial precursor solution. The significant depletion of Co in the detached material strongly suggests that cobalt was preferentially leached from the electrode structure prior to the onset of mechanical detachment. This finding supports the hypothesis that early stage Co dissolution contributes to structural destabilization and reduced long-term durability of NiCoO$_x$ electrodes under dynamic operating conditions.

Ultimately, the degradation stages and underlying mechanisms of the NiCoOx OER catalyst under repeated start-up/shut-down ADT cycles were systematically elucidated in the present study. These findings are schematically summarized in Figure 6, providing a comprehensive visual representation of the sequential compositional and structural changes leading to catalyst deterioration.

4. CONCLUSION

The start-up/shut-down accelerated durability test (ADT) protocol was applied to a NiCoO$_x$ oxygen evolution reaction (OER) catalyst to simulate the dynamic operation of renewable energy sources (RESs). The protocol consisted of two phases: a steady-state operation phase at a constant current density of 0.6 A cm^{-2} for 60 s, followed by a shut-down phase, during which the electrode was held at constant potentials of 0.3, 0.5, 0.7, or 1.3 V for another 60 s. The shut-down potentials were selected based on reverse current experiments and represent the lowest anode potential observed after prolonged reverse current flow in a bipolar plate AWE (alkaline water electrolyzer) stack. The study found that the severity of degradation increased as the shut-down potential decreased relative to the electrode's open-circuit potential. Moreover, the duration of the shut-down phase played a significant role in determining the degradation rate, as sufficient time was required for the complete reduction of the anodic material. Compared to the conventional cyclic voltammetry-based ADT (CV-ADT) protocol employed as a reference in this study, the start-up/shut-down protocol more effectively captured degradation behavior characteristic of intermittent operation, while also offering a time-efficient evaluation approach. The findings from the ADT experiments in this study highlighted the critical need to adapt accelerated stability assessments that accurately reflect real-world electrolysis conditions, ensuring more reliable and practical evaluations for long-term performance.

X-ray absorption spectroscopy (XAS) measurements confirmed that Ni ions functioned as the primary active sites for the OER, while Co ions exhibited a synergistic effect, enhancing overall catalytic activity. However, with continued ADT cycling, preferential leaching of Co ions occurred, leading to structural weakening and collapse of the near-surface material framework. This degradation ultimately caused a significant loss of catalytic material and diminished OER performance.

■ ASSOCIATED CONTENT

Supporting Information

The Supporting Information is available free of charge at https://pubs.acs.org/doi/10.1021/acsami.5c10518.

Additional electrochemical data (electrode potential over ADT cycles and CV of the electrode before and after the ADT at different conditions), XRD spectra of NiCoO$_x$/Ni mesh electrode, unnormalized TEY spectra, PFY spectra, XPS spectra during ADT cycling, and complementary figures illustrating catalyst morphology under different ADT cycles (PDF)

https://doi.org/10.1021/acsami.5c10518
ACS Appl. Mater. Interfaces 2025, 17, 61929–61940

AUTHOR INFORMATION

Corresponding Author

Ashraf Abdel Haleem − *Institute of Advanced Sciences, Yokohama National University, Yokohama 240-8501, Japan;* orcid.org/0000-0002-9656-6724; Email: hassan-ashraf-xj@ynu.ac.jp

Authors

Hayato Enjoji − *Graduate School of Engineering Science, Yokohama National University, Yokohama 240-8501, Japan*

Kyounghee Gu − *Graduate School of Engineering Science, Yokohama National University, Yokohama 240-8501, Japan*

Takuto Miwa − *Graduate School of Engineering Science, Yokohama National University, Yokohama 240-8501, Japan*

Yoshiyuki Kuroda − *Graduate School of Engineering Science, Yokohama National University, Yokohama 240-8501, Japan;* orcid.org/0000-0001-6095-0313

Yuki Orikasa − *Department of Applied Chemistry, Ritsumeikan University, Shiga 525-8577, Japan;* orcid.org/0000-0002-9869-9520

Tomoki Uchiyama − *Graduate School of Human and Environmental Studies, Kyoto University, Kyoto 606-8501, Japan;* Present Address: Department of Material Science, Faculty of Engineering, Tohoku University, 6-6 Aza-Aoba, Aramaki, Sendai, Aoba-ku, Miyagi 980-8579, Japan; orcid.org/0000-0003-4880-7498

Yoshiharu Uchimoto − *Graduate School of Human and Environmental Studies, Kyoto University, Kyoto 606-8501, Japan;* orcid.org/0000-0002-1491-2647

Shigenori Mitsushima − *Institute of Advanced Sciences, Yokohama National University, Yokohama 240-8501, Japan; Graduate School of Engineering Science, Yokohama National University, Yokohama 240-8501, Japan*

Complete contact information is available at: https://pubs.acs.org/10.1021/acsami.5c10518

Notes

The authors declare no competing financial interest.

ACKNOWLEDGMENTS

This research was supported by P14021 and JPNP 20003 project funds that were commissioned by the New Energy and Industrial Technology Development Organization (NEDO).

REFERENCES

(1) Pramuanjaroenkij, A.; Kakaç, S. The Fuel Cell Electric Vehicles: The Highlight Review. *Int. J. Hydrogen Energy* **2023**, *48*, 9401−9425.

(2) Hwang, J.; Maharjan, K.; Cho, H. J. A Review of Hydrogen Utilization in Power Generation and Transportation Sectors: Achievements and Future Challenges. *Int. J. Hydrogen Energy* **2023**, *48*, 28629−28648, DOI: 10.1016/j.ijhydene.2023.04.024.

(3) Guan, D.; Wang, B.; Zhang, J.; Shi, R.; Jiao, K.; Li, L.; Wang, Y.; Xie, B.; Zhang, Q.; Yu, J.; Zhu, Y.; Shao, Z.; Ni, M. Hydrogen Society: From Present to Future. *Energy Environ. Sci.* **2023**, *16*, 4926−4943, DOI: 10.1039/d3ee02695g.

(4) Mazzeo, D.; Herdem, M. S.; Matera, N.; Wen, J. Z. Green Hydrogen Production: Analysis for Different Single or Combined Large-Scale Photovoltaic and Wind Renewable Systems. *Renewable Energy* **2022**, *200*, 360−378.

(5) Yang, X.; Nielsen, C. P.; Song, S.; McElroy, M. B. Breaking the Hard-to-Abate Bottleneck in China's Path to Carbon Neutrality with Clean Hydrogen. *Nat. Energy* **2022**, *7* (10), 955−965.

(6) Timilsina, G. R. Are Renewable Energy Technologies Cost Competitive for Electricity Generation? *Renewable Energy* **2021**, *180*, 658−672.

(7) Blakers, A.; Stocks, M.; Lu, B.; Cheng, C. The Observed Cost of High Penetration Solar and Wind Electricity. *Energy* **2021**, *233*, No. 121150.

(8) van der Zwaan, B.; Fattahi, A.; Dalla Longa, F.; Dekker, M.; van Vuuren, D.; Pietzcker, R.; Rodrigues, R.; Schreyer, F.; Huppmann, D.; Emmerling, J.; Pfenninger, S.; Lombardi, F.; Fragkos, P.; Kannavou, M.; Fotiou, T.; Tolios, G.; Usher, W. Electricity- and Hydrogen-Driven Energy System Sector-Coupling in Net-Zero CO2 Emission Pathways. *Nat. Commun.* **2025**, *16* (1), No. 1368.

(9) Ozturk, M.; Dincer, I. A Comprehensive Review on Power-to-Gas with Hydrogen Options for Cleaner Applications. *Int. J. Hydrogen Energy* **2021**, *46*, 31511−31522, DOI: 10.1016/j.ijhydene.2021.07.066.

(10) Abdel Haleem, A.; Nagasawa, K.; Kuroda, Y.; Nishiki, Y.; Zaenal, A.; Mitsushima, S. A New Accelerated Durability Test Protocol for Water Oxidation Electrocatalysts of Renewable Energy Powered Alkaline Water Electrolyzers. *Electrochemistry* **2021**, *89* (2), 186−191.

(11) Kim, J. E.; Kim, T. H.; Park, C. S.; Jung, K.; Yoon, J.; Lee, K. B.; Kang, K. S. Probing the (de)Activation of Raney Nickel−Iron Anodes during Alkaline Water Electrolysis by Accelerated Deactivation Testing. *Electrochem. Commun.* **2023**, *157*, No. 107601.

(12) Kojima, H.; Nagasawa, K.; Todoroki, N.; Ito, Y.; Matsui, T.; Nakajima, R. Influence of Renewable Energy Power Fluctuations on Water Electrolysis for Green Hydrogen Production. *Int. J. Hydrogen Energy* **2023**, *48*, 4572−4593, DOI: 10.1016/j.ijhydene.2022.11.018.

(13) Uchino, Y.; Kobayashi, T.; Hasegawa, S.; Nagashima, I.; Sunada, Y.; Manabe, A.; Nishiki, Y.; Mitsushima, S. Relationship Between the Redox Reactions on a Bipolar Plate and Reverse Current After Alkaline Water Electrolysis. *Electrocatalysis* **2018**, *9* (1), 67−74.

(14) Uchino, Y.; Kobayashi, T.; Hasegawa, S.; Nagashima, I.; Sunada, Y.; Manabe, A.; Nishiki, Y.; Mitsushima, S. Dependence of the Reverse Current on the Surface of Electrode Placed on a Bipolar Plate in an Alkaline Water Electrolyzer. *Electrochemistry* **2018**, *86* (3), 138−144.

(15) Guruprasad, N.; van der Schaaf, J.; de Groot, M. T. Unraveling the Impact of Reverse Currents on Electrode Stability in Anion Exchange Membrane Water Electrolysis. *J. Power Sources* **2024**, *613*, No. 234877.

(16) Abdel Haleem, A.; Huyan, J.; Nagasawa, K.; Kuroda, Y.; Nishiki, Y.; Kato, A.; Nakai, T.; Araki, T.; Mitsushima, S. Effects of Operation and Shutdown Parameters and Electrode Materials on the Reverse Current Phenomenon in Alkaline Water Analyzers. *J. Power Sources* **2022**, *535*, No. 231454.

(17) Kuroda, Y.; Mizukoshi, D.; Yadav, V.; Taniguchi, T.; Sasaki, Y.; Nishiki, Y.; Awaludin, Z.; Kato, A.; Mitsushima, S. Integration of Multifunctionality in a Colloidal Self-Repairing Catalyst for Alkaline Water Electrolysis to Achieve High Activity and Durability. *Adv. Energy Sustainable Res.* **2024**, *5*, No. 2400196.

(18) Kuroda, Y.; Nishimoto, T.; Mitsushima, S. Self-Repairing Hybrid Nanosheet Anode Catalysts for Alkaline Water Electrolysis Connected with Fluctuating Renewable Energy. *Electrochim. Acta* **2019**, *323*, No. 134812.

(19) Kim, Y.; Jung, S. M.; Kim, K. S.; Kim, H. Y.; Kwon, J.; Lee, J.; Cho, H. S.; Kim, Y. T. Cathodic Protection System against a Reverse-Current after Shut-Down in Zero-Gap Alkaline Water Electrolysis. *JACS Au* **2022**, *2* (11), 2491−2500.

(20) Jung, S. M.; Kim, Y.; Lee, B. J.; Jung, H.; Kwon, J.; Lee, J.; Kim, K. S.; Kim, Y. W.; Kim, K. J.; Cho, H. S.; Park, J. H.; Han, J. W.; Kim, Y. T. Reverse-Current Tolerance for Hydrogen Evolution Reaction Activity of Lead-Decorated Nickel Catalysts in Zero-Gap Alkaline Water Electrolysis Systems. *Adv. Funct. Mater.* **2024**, *34* (27), No. 2316150.

(21) Marquez, R. A.; Espinosa, M.; Kalokowski, E.; Son, Y. J.; Kawashima, K.; Le, T. V.; Chukwuneke, C. E.; Mullins, C. B. A Guide to Electrocatalyst Stability Using Lab-Scale Alkaline Water Electrolyzers. *ACS Energy Lett.* **2024**, *9*, 547−555, DOI: 10.1021/acsenergylett.3c02758.

(22) Longden, T.; Beck, F. J.; Jotzo, F.; Andrews, R.; Prasad, M. 'Clean' Hydrogen? − Comparing the Emissions and Costs of Fossil

Fuel versus Renewable Electricity Based Hydrogen. *Appl. Energy* **2022**, *306*, No. 118145.
(23) Yagmur Goren, A.; Dincer, I.; Khalvati, A. A Comprehensive Review on Environmental and Economic Impacts of Hydrogen Production from Traditional and Cleaner Resources. *J. Environ. Chem. Eng.* **2023**, *11*, No. 111187, DOI: 10.1016/j.jece.2023.111187.
(24) Dobó, Z.; Palotás, Á. B. Impact of the Current Fluctuation on the Efficiency of Alkaline Water Electrolysis. *Int. J. Hydrogen Energy* **2017**, *42* (9), 5649−5656.
(25) Ehlers, J. C.; Feidenhans'l, A. A.; Therkildsen, K. T.; Larrazábal, G. O. Affordable Green Hydrogen from Alkaline Water Electrolysis: Key Research Needs from an Industrial Perspective. *ACS Energy Lett.* **2023**, *8*, 1502−1509, DOI: 10.1021/acsenergylett.2c02897.
(26) Mitsushima, S.; Ioroi, T.; Kuroda , .; Nagasawa, K.; Uchiyama, T.; Orikasa, Y.; Inoue, H.; Higuchi, E.; Ando, K.; Nakajima, T.; Misumi, R.; Uchimoto, Y. Measurement Methods on Electrodes and Electrocatalysts for Water Electrolysis. *Electrochemistry* **2025**, *93*, No. 046001.
(27) Timoshenko, J.; Roldan Cuenya, B. In Situ/ Operando Electrocatalyst Characterization by X-Ray Absorption Spectroscopy. *Chem. Rev.* **2021**, *121*, 882−961, DOI: 10.1021/acs.chemrev.0c00396.
(28) Drevon, D.; Görlin, M.; Chernev, P.; Xi, L.; Dau, H.; Lange, K. M. Uncovering The Role of Oxygen in Ni-Fe(OxHy) Electrocatalysts Using In Situ Soft X-Ray Absorption Spectroscopy during the Oxygen Evolution Reaction. *Sci. Rep.* **2019**, *9* (1), No. 1532, DOI: 10.1038/s41598-018-37307-x.
(29) Rangachary, M. Accelerated Stress Test (AST) Development for Advanced Liquid Alkaline Water Electrolysis 2022 https://www.energy.gov/sites/default/files/2022-02/6-ASTs-LiquidAlkalineWorkshop.pdf.
(30) Todoroki, N.; Nagasawa, K.; Enjoji, H.; Mitsushima, S. Suppression of Catalyst Layer Detachment by Interfacial Microstructural Modulation of the NiCo2O4/Ni Oxygen Evolution Electrode for Renewable Energy-Powered Alkaline Water Electrolysis. *ACS Appl. Mater. Interfaces* **2023**, *15* (20), 24399−24407.
(31) Yang, Q.; Choi, H.; Al-Abed, S. R.; Dionysiou, D. D. Iron-Cobalt Mixed Oxide Nanocatalysts: Heterogeneous Peroxymonosulfate Activation, Cobalt Leaching, and Ferromagnetic Properties for Environmental Applications. *Appl. Catal., B* **2009**, *88* (3−4), 462−469.
(32) Wang, H. Y.; Hsu, Y. Y.; Chen, R.; Chan, T. S.; Chen, H. M.; Liu, B. Ni3+-Induced Formation of Active NiOOH on the Spinel Ni-Co Oxide Surface for Efficient Oxygen Evolution Reaction. *Adv. Energy Mater.* **2015**, *5* (10), No. 1500091.
(33) Acharya, P.; Hong, J.; Manso, R.; Hoffman, A. S.; Kekedy-Nagy, L.; Chen, J.; Bare, S. R.; Greenlee, L. F. Temporal Ni K-Edge X-Ray Absorption Spectroscopy Study Reveals the Kinetics of the Ni Redox Behavior of the Iron-Nickel Oxide Bimetallic OER Catalyst. *J. Phys. Chem. C* **2023**, *127* (25), 11891−11901.
(34) Shi, X.; Bernasek, S. L.; Selloni, A. Oxygen Deficiency and Reactivity of Spinel NiCo2O4 (001) Surfaces. *J. Phys. Chem. C* **2017**, *121* (7), 3929−3937.
(35) Zhao, H.; Zhu, L.; Yin, J.; Jin, J.; Du, X.; Tan, L.; Peng, Y.; Xi, P.; Yan, C. H. Stabilizing Lattice Oxygen through Mn Doping in NiCo2O4-δ Spinel Electrocatalysts for Efficient and Durable Acid Oxygen Evolution. *Angew. Chem., Int. Ed.* **2024**, *63* (20), No. e202402171, DOI: 10.1002/anie.202402171.
(36) Madkhali, M. M. M.; Rankine, C. D.; Penfold, T. J. Enhancing the Analysis of Disorder in X-Ray Absorption Spectra: Application of Deep Neural Networks to T-Jump-X-Ray Probe Experiments †. *Phys. Chem. Chem. Phys.* **2021**, *23*, 9259−9269.
(37) Ali-Löytty, H.; Louie, M. W.; Singh, M. R.; Li, L.; Sanchez Casalongue, H. G.; Ogasawara, H.; Crumlin, E. J.; Liu, Z.; Bell, A. T.; Nilsson, A.; Friebel, D. Ambient-Pressure XPS Study of a Ni-Fe Electrocatalyst for the Oxygen Evolution Reaction. *J. Phys. Chem. C* **2016**, *120* (4), 2247−2253.
(38) Lutterman, D. A.; Surendranath, Y.; Nocera, D. G. A Self-Healing Oxygen-Evolving Catalyst. *J. Am. Chem. Soc.* **2009**, *131* (11), 3838−3839.
(39) Ikeno, H.; Tanaka, I.; Koyama, Y.; Mizoguchi, T.; Ogasawara, K. First-Principles Multielectron Calculations of Ni L2,3 NEXAFS and ELNES for LiNi O2 and Related Compounds. *Phys. Rev. B:Condens. Matter Mater. Phys.* **2005**, *72* (7), No. 075123, DOI: 10.1103/PhysRevB.72.075123.
(40) Qu, Y.; Gomaa, M. M.; Sayed, M. H.; Boshta, M.; Greczynski, G.; Yakimova, R.; Sun, J. A Comparative Study of NiCo2O4, NiO, and Co3O4 Electrocatalysts Synthesized by a Facile Spray Pyrolysis For Electrochemical Water Oxidation. *Adv. Mater. Interfaces* **2024**, *11* (8), No. 2300920, DOI: 10.1002/admi.202300920.
(41) Xia, C.; Li, F. M.; He, C.; Zaman, S.; Guo, W.; Xia, B. Y. Structural Reconstruction of Electrocatalysts *Fundam. Res.* 2024 DOI: 10.1016/j.fmre.2024.04.017, in press.
(42) Speck, F. D.; Zagalskaya, A.; Alexandrov, V.; Cherevko, S. Periodicity in the Electrochemical Dissolution of Transition Metals. *Angew. Chem., Int. Ed.* **2021**, *60* (24), 13343−13349.
(43) Ospina-Acevedo, F. A.; Godínez-Salomón, J. F.; Naymik, Z. G.; Matthews, K. C.; Warner, J. H.; Rhodes, C. P.; Balbuena, P. B. Impacts of Surface Reconstruction and Metal Dissolution on Ru1-XTixO2 Acidic Oxygen Evolution Electrocatalysts. *J. Phys. Chem. C* **2025**, *129*, 3595−3613.
(44) Menezes, P. W.; Indra, A.; Bergmann, A.; Chernev, P.; Walter, C.; Dau, H.; Strasser, P.; Driess, M. Uncovering the Prominent Role of Metal Ions in Octahedral: Versus Tetrahedral Sites of Cobalt-Zinc Oxide Catalysts for Efficient Oxidation of Water. *J. Mater. Chem. A* **2016**, *4* (25), 10014−10022.
(45) Guan, D.; Ryu, G.; Hu, Z.; Zhou, J.; Dong, C. L.; Huang, Y. C.; Zhang, K.; Zhong, Y.; Komarek, A. C.; Zhu, M.; Wu, X.; Pao, C. W.; Chang, C. K.; Lin, H. J.; Chen, C. Te.; Zhou, W.; Shao, Z. Utilizing Ion Leaching Effects for Achieving High Oxygen-Evolving Performance on Hybrid Nanocomposite with Self-Optimized Behaviors. *Nat. Commun.* **2020**, *11* (1), No. 3376.